

Comment on “New Freezeout Mechanism for Strongly Interacting Dark Matter”

Shu-Yu Ho* and Chih-Ting Lu†

Korea Institute for Advanced Study, Seoul 02455, Republic of Korea

In a recent Letter, J. Smirnov and J. F. Beacom [1] proposed a new freezeout mechanism for strongly interacting dark matter (DM) dubbed Co-SIMP, where the reaction rate of the $3 \rightarrow 2$ process, $\chi + \chi + \text{sm} \rightarrow \bar{\chi} + \text{sm}$ with χ the Co-SIMP DM and sm the standard model (SM) particle, determines the relic abundance of DM; see the left graph in Fig. 1. In their work, they consider two cases for the Co-SIMP masses : (i) the typical case, $m_\chi \ll m_{\text{sm}}$, and (ii) the edge case, $m_\chi \simeq m_{\text{sm}}$, where m_χ and m_{sm} are the Co-SIMP and SM particle masses, respectively. Here we want to comment on case (ii).

As we have learned in our recent study [2], any five-point interaction attaching different DM species or SM particles can always generate a two-loop $2 \rightarrow 2$ process that would enforce the heavier particles annihilate into the lighter particles; see the right graph of Fig. 1. Intuitively, one may think this process is suppressed by the two-loop factor and can be neglected in comparison to the $3 \rightarrow 2$ process. However, since the $3 \rightarrow 2$ process in the Co-SIMP scenario has to capture one extra nonrelativistic SM particle whose number yield is Boltzmann-suppressed, the reaction rate of the $2 \rightarrow 2$ process may dominate over or be comparable with that of the $3 \rightarrow 2$ process at the chemical freezeout of DM. Note that in Ref. [1], they do notice this two-loop diagram; however, what they concern about is the sensitivity of the elastic scattering cross section between DM and electron to the current and future direct detection experiments.

To illustrate our point explicitly, here we consider an electrophilic model in Ref. [1], where the Co-SIMP DM couples to the electron field, e . The effective operators describing the $3 \rightarrow 2$ and two-loop induced $2 \rightarrow 2$ processes are given by

$$\mathcal{O}_{3 \rightarrow 2} = \frac{1}{3! \Lambda^2} \chi^3 \bar{e} e, \quad \mathcal{O}_{2 \rightarrow 2} = \frac{c_{\chi e}}{\Lambda} \bar{\chi} \chi \bar{e} e, \quad (1)$$

where Λ being the cutoff scale, and $c_{\chi e}$ is the dimensionless loop-induced coupling of the form computed in Ref. [1]. With these interactions, we then calculate the annihilation cross sections for all possible $3 \rightarrow 2$ processes, $\chi\chi\chi \rightarrow e^+e^-$, $\chi\chi e^\pm \rightarrow \bar{\chi}e^\pm$ and $\chi e^+e^- \rightarrow \bar{\chi}\bar{e}$, as well as $2 \rightarrow 2$ processes, $\chi\bar{\chi} \rightarrow e^+e^-$ and $e^+e^- \rightarrow \chi\bar{\chi}$, and derive the Boltzmann equation of the number density for χ . We summarize them in the appendix. After numerically solving the Boltzmann equation, we obtain the result as shown in Fig. 2, where color curves satisfy the observed DM relic density. As indicated, the cutoff scale is enhanced by a factor of $2 \sim 3$ depending on the Co-SIMP mass. Therefore, the $2 \rightarrow 2$ process does

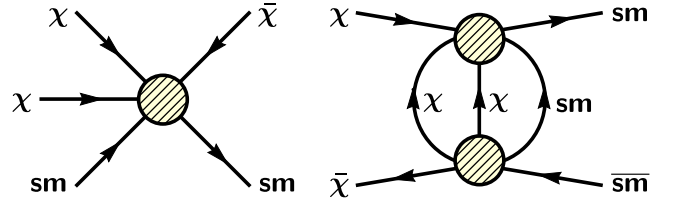


FIG. 1. Feynman diagrams of the $3 \rightarrow 2$ and $2 \rightarrow 2$ processes in the Co-SIMP paradigm.

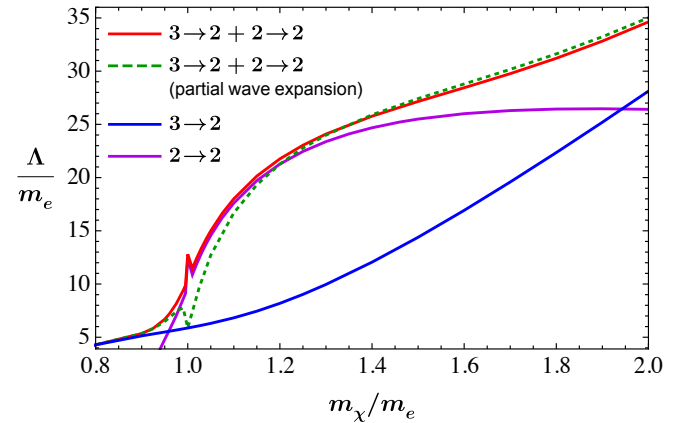


FIG. 2. Cutoff scale versus Co-SIMP mass in the edge case, where the red curve corresponds to the case with both $3 \rightarrow 2$ and $2 \rightarrow 2$ processes, and the blue (purple) curve corresponds to the case with only $3 \rightarrow 2$ ($2 \rightarrow 2$) processes, and the green dashed curve utilizes the $2 \rightarrow 2$ annihilation cross sections in partial wave expansion.

affect the thermal history of the Co-SIMP DM for the edge case. In particular, we find that the reaction rate of the $2 \rightarrow 2$ process is dominated in the mass range $1 \lesssim m_\chi/m_e \lesssim 1.6$, and becomes subdominant in the mass range $1.6 \lesssim m_\chi/m_e \lesssim 2$. In addition, our numerical calculation shows that the freezeout temperature of the Co-SIMP DM is around $x_{\text{f.o.}} \simeq 14 \sim 16$ which is bigger than the estimate in Ref. [1], where $x_{\text{f.o.}} \simeq 10$; see the figures in the appendix.

Finally, let us point out that the relative interaction strengths of $3 \rightarrow 2$ and $2 \rightarrow 2$ processes may depend on UV completion models. One just keeps in mind that the $2 \rightarrow 2$ processes may give some effects on the Co-SIMP mechanism, especially for the edge case.

The authors want to thank Pyungwon Ko for discussion. This work is supported by KIAS Individual Grants under Grant No. PG081201 (S.Y.H.), and No. PG075301 (C.T.L.).

APPENDIX

The full Boltzmann equation of the comoving number density Y_χ for the Co-SIMP, χ , including the $3 \rightarrow 2$ and $2 \rightarrow 2$ processes and assuming no asymmetry between χ and $\bar{\chi}$ in the electrophilic model is given by

$$\begin{aligned} \frac{dY_\chi}{dx} = & -\frac{s^2}{Hx} \left\{ 12 \langle \sigma v^2 \rangle_{\chi\chi\chi \rightarrow e^+e^-} \left[Y_\chi^3 - (Y_\chi^{\text{eq}})^3 \right] \right. \\ & + 2 \langle \sigma v^2 \rangle_{\chi\chi e^+ \rightarrow \bar{\chi}e^+} Y_\chi Y_e^{\text{eq}} (Y_\chi - Y_\chi^{\text{eq}}) \\ & + 2 \langle \sigma v^2 \rangle_{\chi\chi e^- \rightarrow \bar{\chi}e^-} Y_\chi Y_e^{\text{eq}} (Y_\chi - Y_\chi^{\text{eq}}) \\ & \left. - \langle \sigma v^2 \rangle_{\chi e^+e^- \rightarrow \bar{\chi}\bar{\chi}} Y_\chi (Y_e^{\text{eq}})^2 \left(1 - \frac{Y_\chi}{Y_\chi^{\text{eq}}} \right) \right\} \\ & - \frac{s}{Hx} \left\{ 4 \langle \sigma v \rangle_{\chi\bar{\chi} \rightarrow e^+e^-} \left[Y_\chi^2 - (Y_\chi^{\text{eq}})^2 \right] \right. \\ & \left. - \langle \sigma v \rangle_{e^+e^- \rightarrow \chi\bar{\chi}} (Y_e^{\text{eq}})^2 \left[1 - \frac{Y_\chi}{(Y_\chi^{\text{eq}})^2} \right] \right\}, \quad (2) \end{aligned}$$

where $x \equiv m_\chi/T$ is the dimensionless time variable, Y_i^{eq} is the equilibrium comoving number yield of the species i with the internal degrees of freedom g_i [3],

$$Y_i^{\text{eq}} = \frac{45}{4\pi^4} \frac{g_i}{g_{*s}(x)} \left(\frac{m_i x}{m_\chi} \right)^2 K_2 \left(\frac{m_i x}{m_\chi} \right), \quad (3)$$

and s and H are the comoving entropy density and the Hubble parameter, respectively, given by

$$s = \frac{2\pi^2}{45} g_{*s}(x) \frac{m_\chi^3}{x^3}, \quad H = \sqrt{\frac{\pi^2 g_*(x)}{90}} \frac{m_\chi^2}{x^2 m_{\text{Pl}}} \quad (4)$$

with $g_*(g_{*s})$ being the effective energy (entropy) degrees of freedom of the thermal bath [4] and m_{Pl} the reduced Planck mass. Using the interactions in Eq. (1), the $3 \rightarrow 2$ annihilation cross sections are calculated as

$$\begin{aligned} \langle \sigma v^2 \rangle_{\chi\chi\chi \rightarrow e^+e^-} &= \frac{3}{256\pi m_\chi \Lambda^4} \left(1 - \frac{4m_e^2}{9m_\chi^2} \right)^{3/2}, \\ \langle \sigma v^2 \rangle_{\chi\chi e^\pm \rightarrow \bar{\chi}e^\pm} &= \frac{\sqrt{3}}{128\pi m_\chi \Lambda^4} \frac{m_\chi^2 + 2m_\chi m_e + 2m_e^2}{(m_\chi + m_e)(2m_\chi + m_e)^2} \\ &\quad \times \sqrt{3m_\chi^2 + 8m_\chi m_e + 4m_e^2}, \\ \langle \sigma v^2 \rangle_{\chi e^+e^- \rightarrow \bar{\chi}\bar{\chi}} &= \mathcal{O}(x^{-1}), \quad (5) \end{aligned}$$

here we have used the cross section formula of the $3 \rightarrow 2$ process, $1 + 2 + 3 \rightarrow 4 + 5$, in the non-relativistic limit as

$$\begin{aligned} (\sigma v^2)_{123 \rightarrow 45} &\approx \frac{\sqrt{\mathcal{K}[(m_1 + m_2 + m_3)^2, m_4^2, m_5^2]}}{64\pi m_1 m_2 m_3 (m_1 + m_2 + m_3)^2} \\ &\quad \times |\mathcal{M}_{123 \rightarrow 45}|^2, \quad (6) \end{aligned}$$

$$\mathcal{K}(a, b, c) = a^2 + b^2 + c^2 - 2(ab + bc + ac). \quad (7)$$

Notice that the matrix element squared in Eq. (6) is the one defining in the Boltzmann equation with averaging

over initial and final spins, and including appropriate symmetry factors for identical particles in the initial or final states [5]. On the other hand, we employ the following Mandelstam variables in the nonrelativistic limit to evaluate the matrix element squared,

$$s_{jk} = (p_j + p_k)^2 \approx (m_j + m_k)^2, \quad (8)$$

$$s_{45} = (p_4 + p_5)^2 \approx (m_1 + m_2 + m_3)^2, \quad (9)$$

$$t_{k\ell} = (p_k - p_\ell)^2 \approx (m_k - m_\ell)^2 - \frac{2m_k \mu_{45} \Delta m}{m_\ell} \quad (10)$$

with $j, k = \{1, 2, 3\}$, $\ell = \{4, 5\}$ and

$$\mu_{45} = \frac{m_4 m_5}{m_4 + m_5}, \quad (11)$$

$$\Delta m = m_1 + m_2 + m_3 - m_4 - m_5, \quad (12)$$

and these Mandelstam variables satisfy the relation

$$\begin{aligned} & s_{12} + s_{13} + s_{23} + s_{45} \\ & + t_{14} + t_{24} + t_{34} + t_{15} + t_{25} + t_{35} \\ & = 3(m_1^2 + m_2^2 + m_3^2 + m_4^2 + m_5^2). \quad (13) \end{aligned}$$

Also, the thermally-averaged $2 \rightarrow 2$ annihilation cross sections are calculated as [3]

$$\begin{aligned} \langle \sigma v \rangle_{\chi\bar{\chi} \rightarrow e^+e^-} &= \frac{x}{8m_\chi^5 [K_2(x)]^2} \\ &\quad \times \int_{4m_e^2}^{\infty} ds_\chi \sqrt{s_\chi} (s_\chi - 4m_e^2) \\ &\quad \times K_1 \left(\frac{\sqrt{s_\chi} x}{m_\chi} \right) \sigma_{\chi\bar{\chi} \rightarrow e^+e^-}, \quad (14) \end{aligned}$$

$$\begin{aligned} \langle \sigma v \rangle_{e^+e^- \rightarrow \chi\bar{\chi}} &= \frac{x}{8m_e^4 m_\chi [K_2(m_e x/m_\chi)]^2} \\ &\quad \times \int_{4m_e^2}^{\infty} ds_e \sqrt{s_e} (s_e - 4m_e^2) \\ &\quad \times K_1 \left(\frac{\sqrt{s_e} x}{m_\chi} \right) \sigma_{e^+e^- \rightarrow \chi\bar{\chi}}, \quad (15) \end{aligned}$$

where $s_\chi = (p_\chi + p_{\bar{\chi}})^2$ and $s_e = (p_{e^+} + p_{e^-})^2$, and

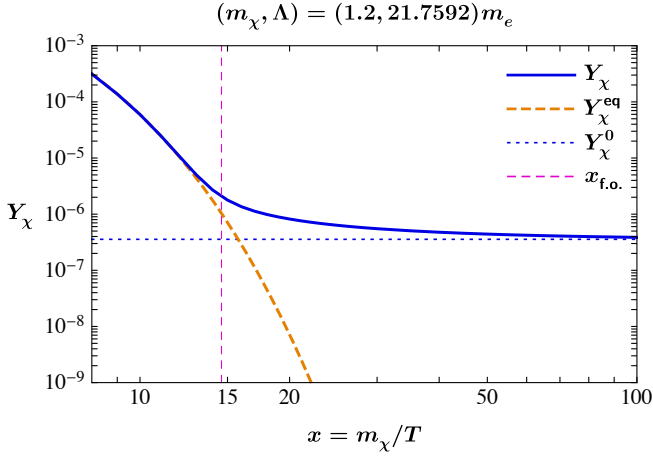
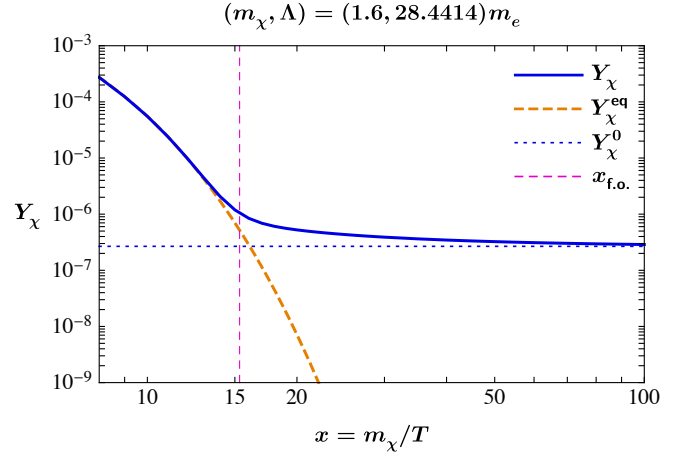
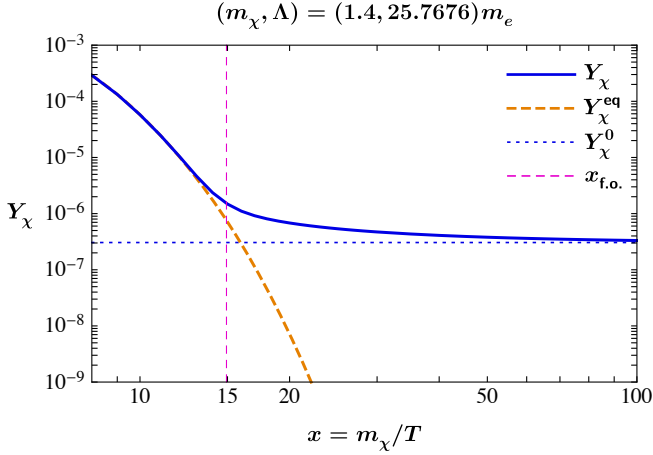
$$\sigma_{\chi\bar{\chi} \rightarrow e^+e^-} = \frac{c_{\chi e}^2}{32\pi\Lambda^2} \frac{(s_\chi - 4m_e^2)^{3/2}}{s_\chi (s_\chi - 4m_\chi^2)^{1/2}}, \quad (16)$$

$$\sigma_{e^+e^- \rightarrow \chi\bar{\chi}} = \frac{c_{\chi e}^2}{32\pi\Lambda^2} \frac{(s_e - 4m_\chi^2)^{1/2} (s_e - 4m_e^2)^{1/2}}{s_e} \quad (17)$$

with [1]

$$c_{\chi e} \approx \frac{m_e}{(4\pi)^4 \Lambda} \left(1 - \frac{m_\chi^2}{\Lambda^2} \right) \ln \left(\frac{\Lambda^2 + m_e^2}{4m_\chi^2} \right). \quad (18)$$

Finally, the prefactor of each cross section in Eq. (2) is the product of the number difference of $\chi/\bar{\chi}$ in the initial and final states and the internal degrees of freedom in the final states [2].

FIG. 3. $Y_\chi(x)$ for $m_\chi = 1.2m_e$ and $1.4m_e$.FIG. 4. $Y_\chi(x)$ for $m_\chi = 1.6m_e$ and $1.8m_e$.

Now, solving Eq. (2) with the proper initial condition $Y_\chi(3 \lesssim x_{\text{ini.}} \ll x_{\text{f.o.}}) = Y_\chi^{\text{eq}}(x_{\text{ini.}})$, we can obtain the cosmological evolution of the comoving number yield of χ as a function of x , $Y_\chi(x)$, and then predict the present density of χ by the relation below [6]

$$\Omega_\chi h^2 \simeq 5.49 \times 10^5 Y_\chi^0 \left(\frac{m_\chi}{\text{MeV}} \right), \quad (19)$$

where $Y_\chi^0 = Y_\chi(x \rightarrow \infty)$. Imposing the observed DM abundance, $\Omega_{\text{DM}} h^2 = 0.12 \pm 0.0012$ [7], one can fix the value of Λ for a given m_χ . We display in Figs. 3 and 4 a few examples of $Y_\chi(x)$ in the mass range of interest, where the Λ values are tuned to fit $\Omega_{\text{DM}} h^2 = 0.12$. As we can see from these figures, the freezeout temperature of the Co-SIMP DM is about $x_{\text{f.o.}} \simeq 14 \sim 16$, where we define the $x_{\text{f.o.}}$ which satisfies the condition $\Delta(x_{\text{f.o.}}) = Y_\chi^{\text{eq}}(x_{\text{f.o.}})$ with $\Delta(x) = Y_\chi(x) - Y_\chi^{\text{eq}}(x)$ [5].

Lastly, let us compare the reaction rates of the $3 \rightarrow 2$ and $2 \rightarrow 2$ processes around the freezeout temperature, the definitions of them are given as follows [5]

$$\Gamma_{\chi\bar{\chi} \rightarrow e^+e^-} \equiv 4 \langle \sigma v \rangle_{\chi\bar{\chi} \rightarrow e^+e^-} n_\chi^{\text{eq}}, \quad (20)$$

$$\Gamma_{\chi\chi\chi \rightarrow e^+e^-} \equiv 12 \langle \sigma v^2 \rangle_{\chi\chi\chi \rightarrow e^+e^-} (n_\chi^{\text{eq}})^2, \quad (21)$$

$$\Gamma_{\chi\chi e^\pm \rightarrow \bar{\chi} e^\pm} \equiv 2 \langle \sigma v^2 \rangle_{\chi\chi e^\pm \rightarrow \bar{\chi} e^\pm} n_\chi^{\text{eq}} n_e^{\text{eq}}, \quad (22)$$

where $n_i^{\text{eq}} = s Y_i^{\text{eq}}$. We show in Fig. 5 the ratios of the reaction rates to the Hubble expansion rate as functions of x around the freezeout temperature with the parameter inputs given in Figs. 3 and 4. Accordingly, the reaction rate of the $2 \rightarrow 2$ process is dominated within the mass range $1 \lesssim m_\chi/m_e \lesssim 1.6$, and is subdominated inside the mass range $1.6 \lesssim m_\chi/m_e \lesssim 2$.

* phyhunter@kias.re.kr

† timluyu@kias.re.kr

- [1] J. Smirnov and J. F. Beacom, Phys. Rev. Lett. **125**, no.13, 131301 (2020).
- [2] S. Y. Ho, P. Ko and C. T. Lu, [arXiv:2107.04375 [hep-ph]].
- [3] P. Gondolo and G. Gelmini, Nucl. Phys. B **360**, 145-179 (1991).
- [4] K. Saikawa and S. Shirai, JCAP **05**, 035 (2018)
- [5] E. W. Kolb and M. S. Turner, Front. Phys. **69**, 1-547 (1990).
- [6] S. Bhattacharya, P. Ghosh and S. Verma, JCAP **01**, 040 (2020).
- [7] N. Aghanim *et al.* [Planck], Astron. Astrophys. **641**, A6 (2020).

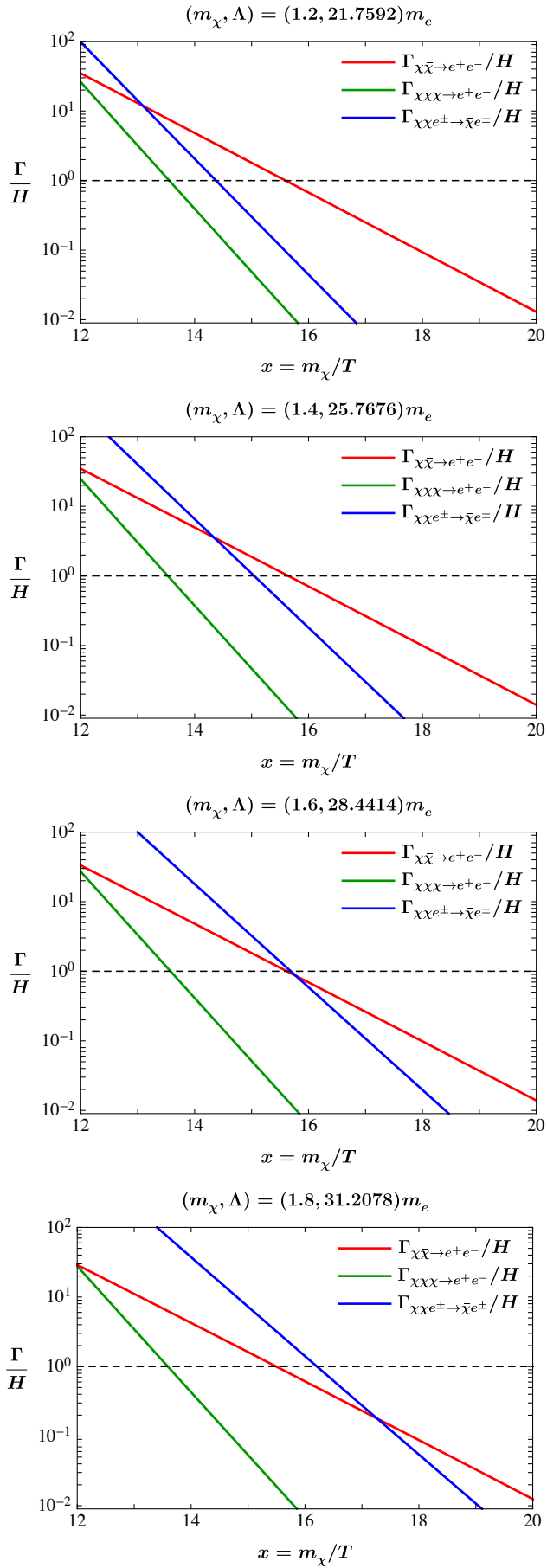


FIG. 5. Γ/H around the $x_{t.o.}$ for $m_e < m_\chi < 2m_e$.